



UNIVERSITY OF LEEDS

This is a repository copy of *Patient-specific parameterised cam geometry in finite element models of femoroacetabular impingement of the hip*.

White Rose Research Online URL for this paper:

<https://eprints.whiterose.ac.uk/128556/>

Version: Accepted Version

Article:

Cooper, RJ orcid.org/0000-0001-5255-1486, Williams, S orcid.org/0000-0002-6963-965X, Mengoni, M orcid.org/0000-0003-0986-2769 et al. (1 more author) (2018) Patient-specific parameterised cam geometry in finite element models of femoroacetabular impingement of the hip. *Clinical Biomechanics*, 54. pp. 62-70. ISSN 0268-0033

<https://doi.org/10.1016/j.clinbiomech.2018.03.007>

© 2018 Published by Elsevier Ltd. This manuscript version is made available under the CC-BY-NC-ND 4.0 license <http://creativecommons.org/licenses/by-nc-nd/4.0/>

Reuse

Items deposited in White Rose Research Online are protected by copyright, with all rights reserved unless indicated otherwise. They may be downloaded and/or printed for private study, or other acts as permitted by national copyright laws. The publisher or other rights holders may allow further reproduction and re-use of the full text version. This is indicated by the licence information on the White Rose Research Online record for the item.

Takedown

If you consider content in White Rose Research Online to be in breach of UK law, please notify us by emailing eprints@whiterose.ac.uk including the URL of the record and the reason for the withdrawal request.



eprints@whiterose.ac.uk
<https://eprints.whiterose.ac.uk/>

1 Patient-specific parameterised cam geometry in finite element models of
2 femoroacetabular impingement of the hip

3

4 Robert J. Cooper, Sophie Williams, Marlène Mengoni, Alison C. Jones

5

6 Institute of Medical and Biological Engineering, School of Mechanical Engineering, University
7 of Leeds, Leeds, LS2 9JT, UK

8

9

10 Corresponding author

11 Robert J. Cooper

12 Institute of Medical and Biological Engineering, School of Mechanical Engineering,

13 University of Leeds,

14 Leeds, LS2 9JT, UK

15 Email: r.j.cooper@leeds.ac.uk

16

17 Word counts

18 Abstract: 245 (limit 250)

19 Main text: 3964 (limit 4000)

20 **ABSTRACT**

21 *Background:* Impingement resulting in soft tissue damage has been observed in hips with
22 abnormal morphologies. Geometric parameterisation can be used to automatically generate
23 a range of bone geometries for use in computational models, including femurs with cam
24 deformity on the femoral neck.

25 *Methods:* This study verified patient-specific parametric finite element models of 20
26 patients with cam deformity (10 female, 10 male) through comparison to their patient-
27 specific segmentation-based equivalents. The parameterisation system was then used to
28 generate further models with parametrically defined geometry to investigate morphological
29 changes in both the femur and acetabulum and their effects on impingement.

30 *Findings:* Similar findings were observed between segmentation-based and parametric
31 models when assessing soft tissue strains under impingement conditions, resulting from
32 high flexion and internal rotations. Parametric models with cam morphology demonstrated
33 that clinically used alpha angles should not be relied on for estimating impingement severity
34 since planar views do not capture the full three-dimensional geometry of the joint.
35 Furthermore, the parametric approach allowed study of labral shape changes, indicating
36 higher strains can result from bony overcoverage.

37 *Interpretation:* The position of cams, as well as their size, can affect the level of soft tissue
38 strain occurring in the hip. This highlights the importance of reporting the full details of
39 three-dimensional geometry used when developing computational models of the hip joint
40 and suggests that it could be beneficial to stratify the patient population when considering
41 treatment options, since certain morphologies may be at greater risk of elevated soft tissue
42 strain.

43

44 **Keywords:** *femoroacetabular impingement; finite element; hip shape; geometric parameterisation*

45

46 **1. INTRODUCTION**

47 Abnormal bone morphology in the hip is associated with femoroacetabular impingement
48 (FAI), in which repeated contact between the proximal femur and the acetabular rim can
49 result in pain and intra-articular damage [1]. A particular example is cam deformity, in which
50 excess bone is present on the femoral neck. Cams most typically occur in young adults, and
51 are more prevalent among males [2]. Understanding of the circumstances leading to
52 symptomatic impingement remains elusive, especially because some hips possessing
53 morphology characteristic of FAI remain asymptomatic [3].

54 In order to investigate the effects of bone morphology on tissue strains computationally, it
55 is useful to be able to automatically generate multiple geometries representative of the
56 population variation. This can be achieved using a parametric approach to finite element
57 models of the hip [4, 5]. A recent study [4] demonstrated that parameterised models could
58 identify differences in contact mechanics between two different subjects with healthy hips
59 across a gait cycle, providing confidence that such models can be used to systematically

60 evaluate the effects of clinically relevant changes in morphology. However, some studies
61 suggest that models with idealised geometry can lead to poor estimates of hip contact
62 stresses [6, 7]. It is therefore important that parametric models are compared with
63 segmented patient-specific models in order to understand the effects of smoothing out local
64 undulations in subject-specific articular geometries. As well as isolating the effects of
65 individual changes, parametric models with simplified articular surfaces can alleviate
66 computational convergence issues [8] reported to occur when using more complex
67 geometry [9].

68 Geometrical variations generated in parametric models must be well defined. Clinically used
69 radiographic measurements such as the alpha angle, which estimates the asphericity of the
70 femoral head, are highly dependent on the two-dimensional radiographic view of the joint
71 and do not capture the full three-dimensional geometry [10, 11]. Alpha angles can therefore
72 be ambiguous and are not well suited to describing geometrical variation.

73 Contact pressures and stresses have been widely used to assess cartilage compression and
74 potential degradation [6, 7, 9, 12], but strains and positional changes in soft tissues,
75 especially the labrum and cartilage-labrum junction, may be more pertinent for improving
76 understanding of when impingement damage may occur. Abutment of the cam against the
77 acetabular rim may result in damage due to cartilage abrasion and translation of the labrum
78 away from the joint [2, 13].

79 The aims of this study were to:

- 80 1) Establish the effect of geometric simplification in finite element models of impingement
81 when assessing labrum displacement and cartilage-labrum junction strain.
- 82 2) Demonstrate the capability of the parameterisation system in distinguishing the effects of
83 cam size and position, beyond what is possible using an alpha angle measurement.
- 84 3) Assess the effects of parametrically varying labrum size and labrum-bone ratio.

85

86 **2. METHODS**

87 We previously developed a geometric parameterisation system capable of representing
88 segmented femurs with cam deformity with root mean squared surface fitting errors in the
89 region of 0.6 mm, allowing isolation of the size and position of cams [10]. The
90 parameterisation method allowed generation of new femoral geometries with the neck
91 region described by ellipses (Fig. 1).

92 **2.1 Segmented vs parametric femoral geometry**

93 Femurs from 10 female and 10 male patients (age range 22-49 years, median 34.5), with
94 clinically diagnosed cam deformity were segmented from CT images (Sensation 16 CT
95 scanner, Siemens, Berlin and Munich, Germany, voxel size: 0.7422 x 0.7422 x 1 mm) using
96 Simpleware ScanIP 7.0 (Synopsys, Mountain View, USA). Ethical approval was granted by the
97 University of Leeds MEEC research ethics committee (MEEC 11-044). A parameterisation

98 method [10] was used to generate an equivalent parametric model for each segmented
99 model (Fig. 2).

100 Simplified geometry representing the acetabulum was created as a spherical cup shape with
101 33% of the surface area of a complete sphere. Spherical acetabular cartilage was included
102 with the acetabular fossa represented by removing a notch from the centre region. The
103 labrum was generated by sweeping a triangular cross section [5, 13] about the circular
104 acetabular rim. This basic acetabular geometry was scaled according to the head radius of
105 each femur to provide a mean cartilage thickness of approximately 1 mm across all models.
106 Let HR denote the femoral head radius of a given model, then the acetabular cartilage
107 thickness was assigned as HR/A where $A = 22.95$ mm, based on the average head radius for
108 the 20 hips. The labrum length was $7HR/25$ mm [5]. In all models, the acetabulum was
109 rotated to simulate a standardised anteversion angle of 20° and centre edge angle of 30° .
110 These angles were chosen based on reported average values for CE and AV angles, including
111 the subjects in this study [5, 10, 14, 15].

112

113 Starting from a 90° flexion position, boundary conditions were used to simulate internal
114 rotation of the femurs up to a maximum of 35° . In all cases, the acetabulum was fixed in
115 place whilst the femur was constrained in translation and rotated to impinge against the
116 labrum. Contact between surfaces was modelled as frictionless with finite sliding and hard
117 contact (linear penalty algorithm). Femurs were by default rotated about their head centre,
118 but in practice this was only successful in six cases. In the other cases, this rotation either
119 caused severe overclosure of the femoral and acetabular surfaces, or did not result in the
120 cam contacting the labrum. In each case the point of rotation was adjusted on the femoral
121 neck axis to optimise for convergence whilst achieving impingement against the labrum
122 without overclosure due to the irregular contact surfaces. The same boundary conditions
123 were used for the segmented and parametric models of each individual patient.

124 Generation of all models was automated in Abaqus 6.14 (Dassault Systèmes, Vélizy-
125 Villacoublay, France) using Python. All FE models were quasi-static analyses, with geometric
126 non-linearity.

127 **2.2 Parametric morphology tests**

128 In order to demonstrate the capability of the parameterisation system, it was used to
129 generate additional parametric models. Boundary conditions in these models simulated
130 flexion from 70° to 90° , followed by up to 35° of internal rotation.

131 Four models were created with parametrically varied femurs. Maintaining a constant head
132 radius of 25 mm, parameters defining the neck region were adjusted to define four
133 variations, featuring two different cam radii (low and high) and two cam positions (anterior
134 and superior). Alpha angles of these four parametric femurs were measured as the angle
135 between the line passing through the femoral neck midpoint and the femoral head centre,
136 and the line from the femoral head centre to the anterior point where the femoral head

137 diverges from spherical. This was done in anterior-posterior (AP) and in cross-table lateral
138 views using ImageJ 1.51k (National Institute of Health, Rockville, USA) [16].

139 A further five models were generated in which the acetabulum was parametrically varied. In
140 these cases the femur was assigned a constant cam radius and position. The base model
141 used the same acetabulum used in the previous models. The four additional cases were:
142 increased labrum length, with unchanged and increased overall coverage; and decreased
143 labrum length, with unchanged and decreased overall coverage.

144 **2.3 Outputs of interest**

145
146 Peak displacements in the labrum and tensile strains (maximum principal logarithmic strain)
147 at the cartilage-labrum junction were recorded throughout the simulations. Maximum
148 displacements occurred at the labral tip and this gave one indication in each case of the
149 severity of impingement as the labrum was deformed by the cam. Tensile strain occurring at
150 the cartilage-labrum junction area was also of interest because this deformation may be a
151 cause of cartilage surface fibre damage. To quantify model agreement, the difference in
152 results between parametric and segmented models was recorded after every 5° of rotation,
153 allowing the root mean squared difference for each specimen to be calculated.

154 **2.4 Material properties**

155
156 In all models in this study, femoral bones and the acetabulum were modelled as rigid bodies
157 [5, 17]. Femoral cartilage was assigned with isotropic linearly elastic material properties ($E =$
158 12MPa , $\nu = 0.4$) [5, 9]. Biphasic cartilage properties were not considered in this study since
159 modelling cartilage as elastic is an appropriate simplification to predict short term contact
160 stresses [18, 19].

161 Acetabular cartilage and the labrum were also modelled as linearly elastic, but were
162 assigned transversely isotropic properties defined according to typical collagen fibril
163 alignment. Collagen fibrils in cartilage are believed to be orientated parallel to the articular
164 surface in outer layers, but perpendicular and anchored to the bone in inner layers [20, 21,
165 22]. Thus the elastic modulus in the direction perpendicular to the articular surface was
166 assigned to be greatest at the base layer (boundary between subchondral bone and
167 cartilage), reduced in the middle layer and lowest at the articular surface. The modulus in
168 the directions perpendicular to the articular surface was assigned to be greatest at the
169 surface, reduced in the middle layer and lowest at the base layer ($E = 9, 12, 15\text{MPa}$
170 respectively). Collagen fibrils in the labrum are believed to be predominantly aligned
171 circumferentially [23, 24], so a greater modulus was assigned in the circumferential
172 direction ($E = 20\text{MPa}$ and 12MPa respectively). In all acetabular cartilage layers and in the
173 labrum, Poisson's ratio was set as $\nu = 0.4$ and the shear modulus G was assigned so that $2G$
174 $= (E_{\text{mean}}) / (1 + \nu)$.

175 **2.5 Mesh generation and sensitivity**

176 Hexahedral meshes were desired for meshing soft tissues because linear tetrahedral
177 elements are stiffer than hexahedral elements, and using tetrahedral elements for contact
178 problems can result in locking, large stress concentrations and poor estimations of contact
179 areas [25]. Quadrilateral meshes were therefore required on bone surfaces. To achieve
180 quadrilateral meshes on segmented bone surfaces, they were exported from ScanIP using
181 the +NURBS module and subsequently meshed within Abaqus. Femoral cartilage layers were
182 produced as orphan hexahedral meshes created by offsetting the meshes on the femoral
183 bone parts (thickness 1 mm). Acetabular cartilage and the labrum were also meshed with
184 hexahedral elements.

185

186 The mesh density adopted was determined after mesh convergence tests. Displacements
187 seen in the models were converged at the mesh density of three elements across the
188 thickness of the acetabular cartilage and labrum, but local strain was more sensitive to mesh
189 resolution. To achieve convergence for all outputs of interest, six elements were used across
190 the thickness of the acetabular cartilage and labrum (that is, two elements for each distinct
191 cartilage layer), resulting in approximately 156,000 elements for the acetabular soft tissue
192 (8-node linear brick, reduced integration, enhanced hourglass control). Only two elements
193 were used across the thickness of the femoral cartilage because outputs from acetabular
194 side were of interest and the femoral cartilage did not affect contact between the bony cam
195 and acetabular-labral junction.

196

197 **3. RESULTS**

198 The data associated with this paper are openly available from the University of Leeds data
199 Repository [26].

200 For the segmented and equivalent parametric models, the range of positions used for the
201 centre of rotation was -2 mm to 4 mm (where positive is more proximal), and the average
202 position was 1.2 mm proximally above the femoral head centre. The level of internal
203 rotation achieved ranged from 23° to 35°. In all models the typical deformation pattern
204 consisted of displacement of the labrum and compression of the cartilage-labrum junction
205 (Fig. 3). Generally similar displacements and strains occurred in the segmented and
206 equivalent parametric models; the range in root mean squared difference in results for the
207 segmented and parametric models was 0.0039 - 0.1292 mm for peak labral displacement
208 and 0.0002 - 0.0134 for peak strain (Fig. 4). For context, displacements peaked at 5.4 mm,
209 and strains peaked at 0.53. The lower levels of agreement occurred when the local fitting
210 errors between the parametric and segmented surfaces in the cam region were larger,
211 particularly > 1 mm. (Fig. 5).

212 High deformation of elements in the cartilage-labrum junction prevented models converging
213 past a certain level of rotation, so for the additional parametric tests, rotation levels where
214 all models converged were used to generate comparison graphs. This was 15° for the

215 models where cam morphology was varied (Fig. 6) and 25° for the models where acetabular
216 rim morphology was varied (Fig. 7).

217 When cam morphology was varied, measured alpha angles did not predict outputs of
218 interest (Fig. 6). In particular, AP alpha angles were unexpectedly higher ($\alpha = 63.4^\circ$, $\alpha =$
219 83.1°) in the cases with no labral displacement occurring at 15° rotation than in cases where
220 labral displacement did occur ($\alpha = 41.5^\circ$, $\alpha = 44.6^\circ$). The cross-table lateral alpha angle was
221 largest ($\alpha = 83.2^\circ$) in the most severe impingement case (peak strain = 0.3793), but did not
222 distinguish between the other models (α range = $61.0^\circ - 68.5^\circ$) where impingement severity
223 varied as a result of cam size and position as defined on the neck ellipses (strain range =
224 0.0283 – 0.0341, displacement range = 0 - 1.52 mm).

225

226 When acetabular rim and labral morphology was varied, an increase to bone coverage had
227 the greatest effect on impingement severity (Fig. 7). A 10% increase in bone (with labrum
228 size decreased to maintain the same overall coverage) increased strain in the cartilage
229 labral-junction from 0.1155 to 0.4053. Increasing labral length by 10% (thus increasing
230 overall coverage) increased labral displacement from 2.76 mm to 3.29 mm, but had little
231 effect on junction strain, which increased from 0.1155 to 0.1253.

232

233 4. DISCUSSION

234 The aims of this study were to validate the use of geometrically parameterised femoral
235 surfaces against segmented equivalents, and to use parametric models to assess key hip
236 shape morphological variations in 3D. Subject-specific parametric models were compared
237 with segmented models and trends in parametric models were found to be largely in
238 agreement with segmented models. Additionally generated parametrically defined femurs
239 demonstrated the issues with relying on 2D alpha angle measures as an indication of
240 impingement severity potential. A simplified labrum geometry allowed rapid investigation of
241 the effects of morphological variations and suggested bony overcoverage can increase
242 impingement severity. High strains at the cartilage-labral junction resulting from direct
243 compression of the cartilage by the cam, rather than the stretching of cartilage as a result of
244 displacement of the labrum, were seen to be the driver of elevated tensile strains in
245 cartilage in the models.

246 4.1 Segmented vs parametric models

247 Similar displacements and strains occurred in the segmented and equivalent parametric
248 models. This suggested that these outputs were relatively insensitive to the local
249 undulations on the articular surface, which were present in the segmented models but
250 smoothed out in the parametric representation. Previous modelling studies have reported
251 elevated contact pressures and stresses in the anterosuperior cartilage and labrum [5, 9,
252 12], matching clinical reports of damage [27]. This corroborates with findings of high strain
253 in the cartilage-labral junction in the models developed in this study.

254 The comparison between segmented and parametric models provided confidence in the
255 results, in that trends and magnitudes present in segmented models were replicated in
256 parametric models. There was no direct validation since there were other simplifications to
257 the models in terms of boundary conditions and material properties. Measurement of
258 impingement risks by the outcome of the FE models should therefore not be understood as
259 absolute risk. Other studies comparing segmented and parameterised models suggested
260 idealised geometry can underestimate contact stresses occurring in the hip [6, 7], but did
261 not specifically investigate geometry related to impingement. In the impingement scenario
262 modelled here, it was possible to identify the underlying cause of differences in model
263 outputs by quantifying poor fitting between the smooth, parametric surfaces and more
264 undulating, segmented surfaces in contact regions.

265 Given the chosen boundary conditions, displacement of the labrum is a result of the position
266 and peak size of the cam. When a poorer fit between the parametric and segmented
267 surfaces at the cam region occurred, impingement contact arose at appreciably smaller
268 rotation angles in the parametric or segmented case, depending on whether the parametric
269 surface over- or under-estimated the radius of the segmented cam. Earlier contact in the
270 model with the larger radius resulted in more displacement of the acetabular soft tissue at
271 lower angles of rotation. When higher labral displacement occurred in the segmented or
272 parametric model, the tensile strain in the cartilage-labrum junction was usually also higher,
273 since the cartilage was both more compressed by the cam and stretched more as a result of
274 the labral displacement. However discrepancies in the local fit between surfaces at the cam
275 region could be such that the labral tip displacement was higher, whilst the cartilage was
276 compressed less and had lower tensile strain. This emphasises that although a low overall
277 geometrical fitting error can be achieved [10], it does not guarantee that the parametric
278 geometry is able to precisely capture the shape of all cams. The fit in localised regions may
279 be poorer than the overall fit, which in the impingement scenario is of particular importance
280 in the cam region (Fig. 5).

281 **4.2 Parametric tests**

282 Models incorporating parametric femoral variations revealed that cams positioned more
283 anteriorly resulted in more severe impingement in the simulated scenario (flexion followed
284 by internal rotation) (Fig. 6). However, the AP alpha angle on both the anterior cam models
285 was lower than those on the superior cam models. AP alpha angles gave the opposite
286 prediction to the severity indicated by the model outputs, because superior cams were
287 more visible in the AP view. In the anterior cam models, the AP alpha angle increased by
288 only 3.3° when the cam radius was increased, but the severity in the model increased
289 dramatically, indicated by an increase in tensile strain in the cartilage-labrum junction from
290 0.03 to 0.38. For superior cams, increasing the cam radius substantially increased the AP
291 alpha angle, but the additional severity observed in the model was less than that seen
292 between the anterior cam models. Thus using an AP alpha angle, it was not possible to
293 predict the severity of impingement.

294 Alpha angles above 55° have been suggested as indicators of cam impingement [15, 28, 29],
295 so the alpha angles generated here were clinically relevant. The cross-table lateral alpha
296 angle was largest in the most severe impingement case (83.2°), but did not however
297 distinguish between the other models, with similar angles (all above 60°, with a range of
298 7.5°) recorded for the three models. The differences in severity predicted by the models
299 were a result of both the extent and the position of the cams defined in 3D measurements.

300 In the acetabular coverage tests, greater bony coverage resulted in increased strain (Fig. 7).
301 The models therefore predicted that elevated bony acetabular coverage likely increases
302 impingement severity for a given level of rotation. Labral displacement appeared to be
303 driven by the position of its tip relative to the cam, rather than overall labral length. The
304 model with increased labrum length but the same overall coverage (less bone), exhibited
305 less strain at the junction, because the bulk of the labrum was located further from the
306 labral tip when impingement was initiated. It has been suggested that in dysplastic hips,
307 labral length may be increased in the weight-bearing zone, potentially compensating for the
308 lack of bony coverage [30]. The results reported here suggest that the increase in coverage
309 caused by this reaction may not increase impingement severity to the same extent as in
310 cases where coverage is elevated due to excess acetabular bone.

311 **4.3 Limitations and challenges**

312 The models in this study suggest direct compression of the cartilage by the cam as the main
313 cause of impingement damage, but it is important to consider limitations which could mean
314 that effect of labral displacement is underemphasised. Soft tissues were not visible in the
315 patient CT scans and as such, femoral cartilage geometry was estimated by expanding the
316 geometry of the bone, providing consistent methodology for parametric and segmented
317 surfaces. In addition, the current method of generating parametric models requires bone
318 segmentation from 3D images. There are clear benefits to being able to take detailed bone
319 measurements from lower radiation dose imaging systems [31]. However, any reduction in
320 image resolution and associated increase in distance between image slices, reduces the
321 precision by which we can establish the cam size and location.

322 Simplified acetabular geometry was chosen for all models in order to facilitate parametric
323 assessment of labral changes, and to mitigate convergence issues that resulted from contact
324 between irregular articular surfaces. It is important to appreciate that significant subject-
325 specific differences also occur on the acetabular side, which could result in altered tissue
326 strains, since the fit of the femoral head into the acetabulum may vary between patients.
327 Parametric study of geometrical changes to the femur here assumed constant acetabular
328 geometry. Whilst parametric study of changes to the labrum was also conducted, the
329 labrum was defined on a circular acetabular rim, and not verified against subject-specific
330 cases as the femurs were. This was because labral tissue could not be segmented from the
331 clinical CT scans. Furthermore, specimen-specific values for acetabular angles were not
332 deemed appropriate for comparing parametric and segmented models, since it was
333 important to ensure a certain degree of impingement occurred in order to compare trends

334 seen in parametric and segmented cases, and the simplification to spherical acetabular
335 geometry meant that adjusting acetabular angles would unnecessarily restrict the possible
336 range of movement that could be simulated.

337 The adopted approach modelled impingement using applied internal rotations from a
338 flexion position. Previously published loading data [32] was deemed inappropriate since FAI
339 patients are younger and have deformities that could result in altered gait patterns. In the
340 segmentation / parametric comparison models, it was important to ensure the same
341 boundary conditions were applied to both models of each individual patient. Femurs were
342 generally rotated about their head centre; in some cases this caused excessive penetration
343 of the femoral and acetabular surfaces, preventing convergence. Therefore the point of
344 rotation was adjusted to optimise for model convergence whilst achieving impingement
345 against the labrum. To ensure a valid comparison, the boundary conditions were always
346 consistent for the parametric and segmented models of each patient. Differences between
347 boundary conditions used for distinct patients however meant that models of different
348 patients were not directly comparable. The use of parametric models (without the
349 restriction of requiring boundary conditions to match a segmented case) mitigates this
350 problem because the smoother surfaces are less prone to these errors. Additional
351 parametric models varying the femur and acetabulum could therefore be developed and
352 were used to assess the effects of individual morphological variations. Even so, high
353 deformation of elements in the cartilage-labrum junction prevents models converging past a
354 certain level of rotation, so results from lower rotation levels were required to compare
355 models exhibiting severe impingement.

356 **4.4 Conclusions**

357 This study has quantified the effects of using parametric geometries when investigating
358 femoroacetabular impingement, by comparison with a gold standard segmentation
359 approach. In a simulation of the impingement scenario, we showed that discrepancies
360 resulted from possible poor local fit in the cam region, but trends in outcomes of interest
361 were similar between modelling methods. While still requiring full 3D segmentation, there is
362 potential to further develop parametric methods to assess impingement severity based only
363 on measures of the neck and acetabulum.

364 The parametric study demonstrated the enhanced capability of a three-dimensional analysis
365 over current clinical measures of planar alpha angles, which are highly dependent on view.
366 Potential for tissue damage was not predicted by alpha angle measures. We previously
367 reported that among the 20 patients included in this study, females were more likely to
368 have cams located in an anterior position, which are less visible in AP radiographs [10]. In
369 the impingement scenarios tested here, anterior cams caused greater levels of soft tissue
370 strain and could therefore result in more severe articular damage. Although cams are more
371 common in males and tend to be more diffuse in females, their position in females could
372 make them more severe.

373 **ACKNOWLEDGEMENTS**

374 This work was funded by the EPSRC (grant number EP/F500513/1) and the ERC (grant
 375 number StG-2012-306615). Models were run using the University of Leeds high
 376 performance computing cluster ARC2.

377

378 **REFERENCES**

- 379 1. Ganz R, Parvizi J, Beck M, Leunig M, Nötzli H, Siebenrock KA. Femoroacetabular
 380 impingement: a cause for osteoarthritis of the hip. *Clinical orthopaedics and related*
 381 *research*. 2003; **417**:112-120.
 382 doi: 10.1097/01.blo.0000096804.78689.c2
- 383 2. Kuhns BD, Weber AE, Levy DM, Wuerz TH. The Natural History of Femoroacetabular
 384 Impingement. *Frontiers in surgery*. 2015; 2:58.
 385 doi: 10.3389/fsurg.2015.00058
- 386 3. Khanna V, Caragianis A, DiPrimio G, Rakhra K, Beaulé PE. Incidence of hip pain in a
 387 prospective cohort of asymptomatic volunteers is the cam deformity a risk factor for
 388 hip pain? *The American journal of sports medicine*. 2014; **42**(4):793-7
 389 doi: 10.1177/0363546513518417.
- 390 4. Hua X, Li J, Wilcox RK, Fisher J, Jones AC, Geometric parameterisation of pelvic bone
 391 and cartilage in contact analysis of the natural hip: An initial study. *Proceedings of*
 392 *the Institution of Mechanical Engineers, Part H: Journal of Engineering in Medicine*.
 393 2015; **229**(8): 570-580.
 394 doi: 10.1016/j.medengphy.2004.12.008
- 395 5. Chegini S, Beck M, Ferguson SJ. The effects of impingement and dysplasia on stress
 396 distributions in the hip joint during sitting and walking: a finite element analysis.
 397 *Journal of Orthopaedic Research*. 2009; **27**(2):195-201.
 398 doi: 10.1002/jor.20747
- 399 6. Gu DY, Hu F, Wei JH, Dai KR, Chen, YZ. Contributions of non-spherical hip joint
 400 cartilage surface to hip joint contact stress. *Engineering in Medicine and Biology*
 401 *Society, EMBC, 2011 Annual International Conference of the IEEE*: 8166-69.
- 402 7. Anderson AE, Ellis BJ, Maas SA, Weiss JA. Effects of idealized joint geometry on finite
 403 element predictions of cartilage contact stresses in the hip. *Journal of biomechanics*.
 404 2010; **43**(7):1351-1357.
 405 doi: 10.1016/j.jbiomech.2010.01.010
- 406 8. Hellwig FL, Tong J, Hussell JG. Hip joint degeneration due to cam impingement: a
 407 finite element analysis. *Computer methods in biomechanics and biomedical*
 408 *engineering*. 2016; **19**(1):41-8.
 409 doi: 10.1080/10255842.2014.983490
- 410 9. Jorge JP, Simões FM, Pires EB, Rego PA, Tavares DG, Lopes DS, Gaspar A. Finite
 411 element simulations of a hip joint with femoroacetabular impingement. *Computer*
 412 *methods in biomechanics and biomedical engineering*. 2014; **17**(11):1275-84.
 413 doi: 10.1080/10255842.2012.744398

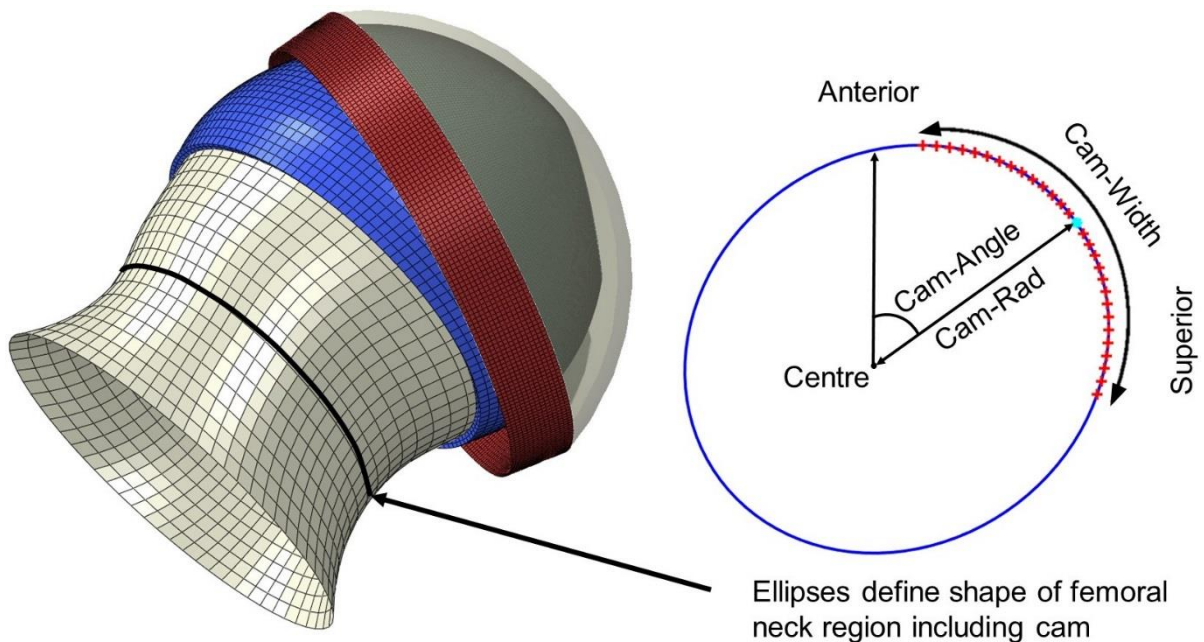
- 414 10. Cooper RJ, Mengoni M, Groves D, Williams S, Bankes MJK, Robinson P, Jones AC.
415 Three-dimensional assessment of impingement risk in geometrically parameterised
416 patient hips compared with clinical measures. *International Journal for Numerical*
417 *Methods in Biomedical Engineering*. 2017; **33**(11):e2867.
418 doi: 10.1002/cnm.2867
- 419 11. Harris MD, Kapron AL, Peters CL, Anderson AE. Correlations between the alpha angle
420 and femoral head asphericity: Implications and recommendations for the diagnosis
421 of cam femoroacetabular impingement. *European journal of radiology*, 2014;
422 **83**(5):788-796.
423 doi: 10.1016/j.ejrad.2014.02.005
- 424 12. Ng KG, Lamontagne M, Labrosse M, Beaulé PE. Hip joint stresses due to cam-type
425 femoroacetabular impingement: a systematic review of finite element simulations.
426 *PloS one*. 2016; **11**(1), e0147813.
427 doi: 10.1371/journal.pone.0147813
- 428 13. Banerjee P, Mclean CR. Femoroacetabular impingement: a review of diagnosis and
429 management. *Current reviews in musculoskeletal medicine*. 2011; **4**(1):23-32.
430 doi: 10.1007/s12178-011-9073-z
- 431 14. Ergen FB, Vudali S, Sanverdi E, Dolgun A, Aydingöz Ü. CT assessment of
432 asymptomatic hip joints for the background of femoroacetabular impingement
433 morphology. *Diagnostic and Interventional Radiology*. 2014; **20**(3), 271.
434 doi: 10.5152/dir.2013.13374
- 435 15. Tannast M, Siebenrock KA, Anderson, SE. Femoroacetabular impingement:
436 radiographic diagnosis—what the radiologist should know. *American Journal of*
437 *Roentgenology*. 2007; **188**(6), 1540-1552.
438 doi: 10.2214/AJR.06.0921
- 439 16. Schindelin J, Arganda-Carreras I, Frise E, Kaynig V, Longair M, Pietzsch T, Preibisch S,
440 Rueden C, Saalfeld S, Schmid B, Tinevez JY. Fiji: an open-source platform for
441 biological-image analysis. *Nature methods*. 2012; **9**(7): 676-682.
442 doi: 10.1038/nmeth.2019
- 443 17. Anderson AE, Ellis BJ, Maas SA, Peters CL, Weiss JA. Validation of finite element
444 predictions of cartilage contact pressure in the human hip joint. *Journal of*
445 *biomechanical engineering*. 2008; **130**(5):051008.
446 doi: 10.1115/1.2953472
- 447 18. Henak CR, Anderson AE, Weiss JA. Subject-specific analysis of joint contact
448 mechanics: application to the study of osteoarthritis and surgical planning. *Journal of*
449 *biomechanical engineering*. 2013; **135**(2):021003.
450 doi: 10.1115/1.4023386
- 451 19. Ateshian GA, Ellis BJ, Weiss JA. Equivalence between short-time biphasic and
452 incompressible elastic material responses. *Journal of biomechanical engineering*.
453 2007; **129**(3):405-12.
454 doi: 10.1115/1.2720918

- 455 20. Sophia Fox AJ, Bedi A, Rodeo SA. The basic science of articular cartilage: structure,
456 composition, and function. *Sports health*. 2009; **1**(6), 461-468.
457 doi: 10.1177/1941738109350438
- 458 21. Meng Q, An S, Damion RA, Jin Z, Wilcox R, Fisher J, Jones A. The effect of collagen
459 fibril orientation on the biphasic mechanics of articular cartilage. *Journal of the*
460 *mechanical behavior of biomedical materials*. 2017; **65**, 439-453.
461 doi: 10.1016/j.jmbbm.2016.09.001
- 462 22. Osawa T, Moriyama S, Tanaka M. Finite element analysis of hip joint cartilage
463 reproduced from real bone surface geometry based on 3D-CT image. *Journal of*
464 *Biomechanical Science and Engineering*. 2014; **9**(2):13-00164.
465 doi: 10.1299/jbse.13-00164
- 466 23. Petersen W, Petersen F, Tillmann B. Structure and vascularization of the acetabular
467 labrum with regard to the pathogenesis and healing of labral lesions. *Archives of*
468 *orthopaedic and trauma surgery*. 2003; **123**(6):283-8.
469 doi: 10.1007/s00402-003-0527-7
- 470 24. Grant AD, Sala DA, Davidovitch RI. The labrum: structure, function, and injury with
471 femoroacetabular impingement. *Journal of children's orthopaedics*. 2012; **6**(5):357-
472 72.
473 doi: 10.1007/s11832-012-0431-1
- 474 25. Maas SA, Ellis BJ, Rawlins DS, Weiss JA. Finite element simulation of articular contact
475 mechanics with quadratic tetrahedral elements. *Journal of biomechanics*. 2016 Mar
476 **21**; **49**(5):659-67.
477 doi: 10.1016/j.jbiomech.2016.01.024
- 478 26. Cooper RJ, Williams S, Mengoni M, Jones AC. Dataset associated with 'Patient-
479 specific parameterised cam geometry in finite element models of femoroacetabular
480 impingement in the hip'. University of Leeds, UK. 2018. [Dataset].
481 <https://doi.org/10.5518/326>
- 482 27. Beck M, Kalhor M, Leunig M, Ganz R. Hip morphology influences the pattern of
483 damage to the acetabular cartilage. *Bone & Joint Journal*. 2005; **87**(7), 012-1018.
484 doi: 10.1302/0301-620X.87B7.15203
- 485 28. Urquhart N, Philippon M, Ye JE, Simunovic N, Ayeni OR. Alpha angle correction in
486 femoroacetabular impingement. *Knee Surgery, Sports Traumatology, Arthroscopy*.
487 2014; **22**(4), 812-821.
488 doi: 10.1007/s00167-013-2678-6
- 489 29. Pfirrmann CW, Mengiardi B, Dora C, Kalberer F, Zanetti M, Hodler J. Cam and pincer
490 femoroacetabular impingement: characteristic MR arthrographic findings in 50
491 patients. *Radiology*. 2006; **240**(3), 778-785.
492 doi: 10.1148/radiol.2403050767
- 493 30. Garabekyan T, Ashwell Z, Chadayammuri V, Jesse MK, Pascual-Garrido C, Petersen B,
494 Mei-Dan O. Lateral acetabular coverage predicts the size of the hip labrum. *The*
495 *American journal of sports medicine*. 2016; **44**(6):1582-9.
496 doi: 10.1177/0363546516634058

- 497 31. Thelen T, Thelen P, Demezon H, Aunoble S, Le Huec JC. Normative 3D acetabular
498 orientation measurements by the low-dose EOS imaging system in 102
499 asymptomatic subjects in standing position: Analyses by side, gender, pelvic
500 incidence and reproducibility. *Orthopaedics & Traumatology: Surgery & Research*.
501 2017; **103**(2):209-15.
502 doi: 10.1016/j.otsr.2016.11.010
- 503 32. Bergmann G, Deuretzbacher G, Heller M, Graichen F, Rohlmann A, Strauss J, Duda
504 GN. Hip contact forces and gait patterns from routine activities. *Journal of*
505 *biomechanics*. 2001; **34**(7):859-71.
506 doi: 10.1016/S0021-9290(01)00040-9

507 FIGURES

508

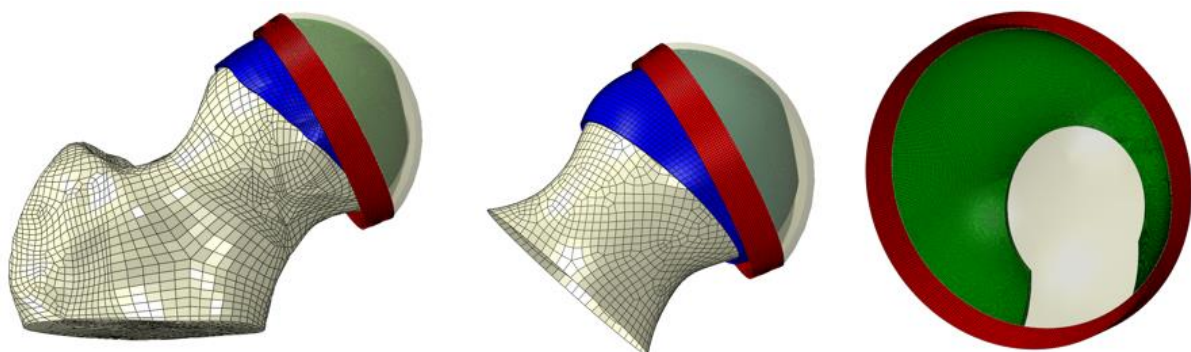


509

510 **Fig 1:** Five ellipses fitted to cross sections of the femoral neck at automatically defined
 511 positions, along with a spherical cap, generated the parametric femoral geometry. The first
 512 four ellipses were linearly spaced between $x/2$ and x , where x is the total number of slices
 513 (rounding these points to integer values). A 5th ellipse was at $HR*1.2$. Cam size and position
 514 was determined by measurements on the 2nd and 3rd ellipses, focusing on the cam region.
 515 Cam angle indicates the position of the cam, whilst radius and width together indicate the
 516 cam extent [10].

517

518

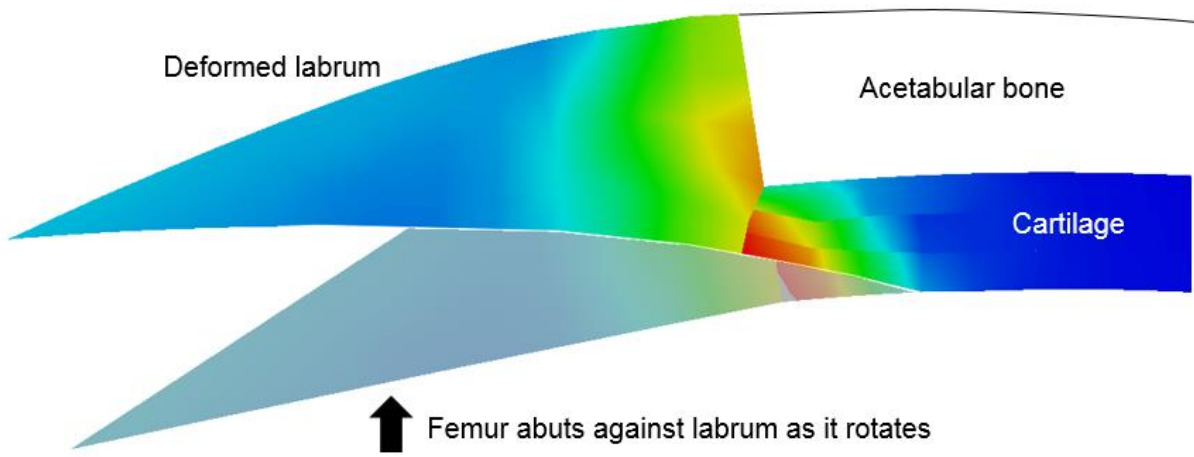


519

520 **Fig 2:** Examples of meshed models showing segmented and parameterised femurs, and the
 521 acetabulum, modelled as rigid surfaces. Femoral cartilage elements are blue, acetabular
 522 labrum elements are red, and acetabular cartilage elements are green.

523

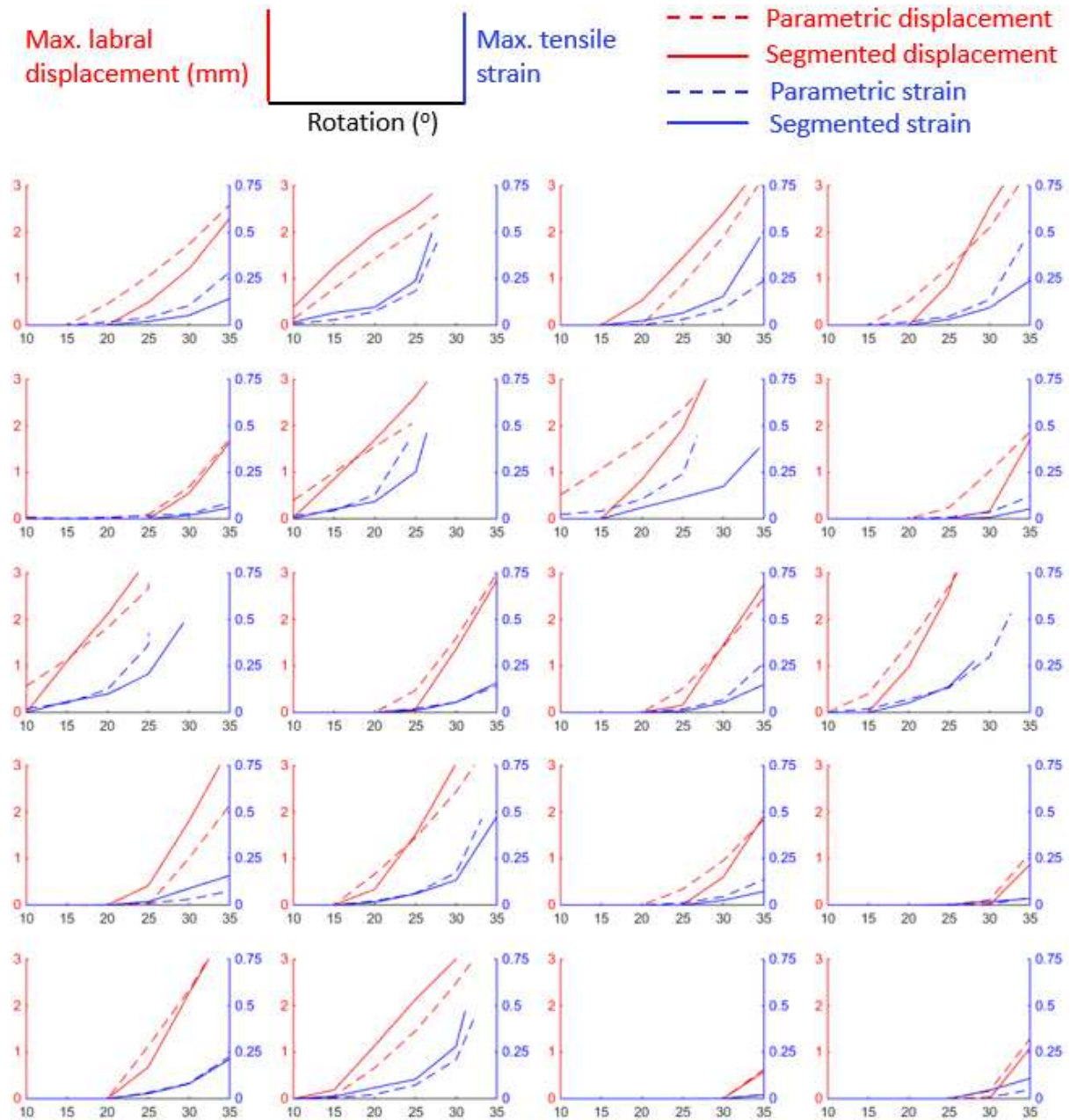
524



525

526 **Fig 3:** Example of a cross-section through a deformed (bright colour) and undeformed
527 (shaded) cartilage-labrum junction. Regions of high tensile strain are displayed in red.

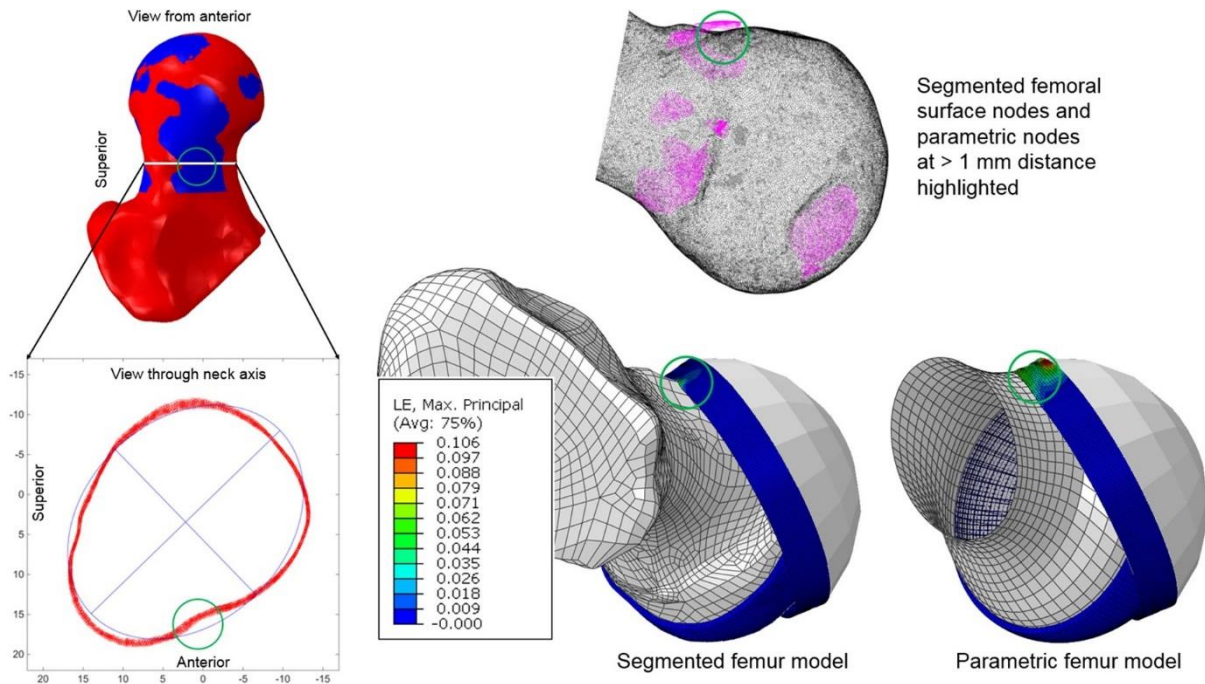
528



529

530 **Fig 4:** Graphs comparing segmented (solid lines) and parametric (dashed lines) models for
 531 each of the 20 cam patients, showing maximum labral displacement (blue, left y-axes, in
 532 mm) and cartilage-labrum junction strain (red, right y-axes as maximum principal
 533 logarithmic strains) with increasing internal rotation of the femur (x-axes, in degrees).

534

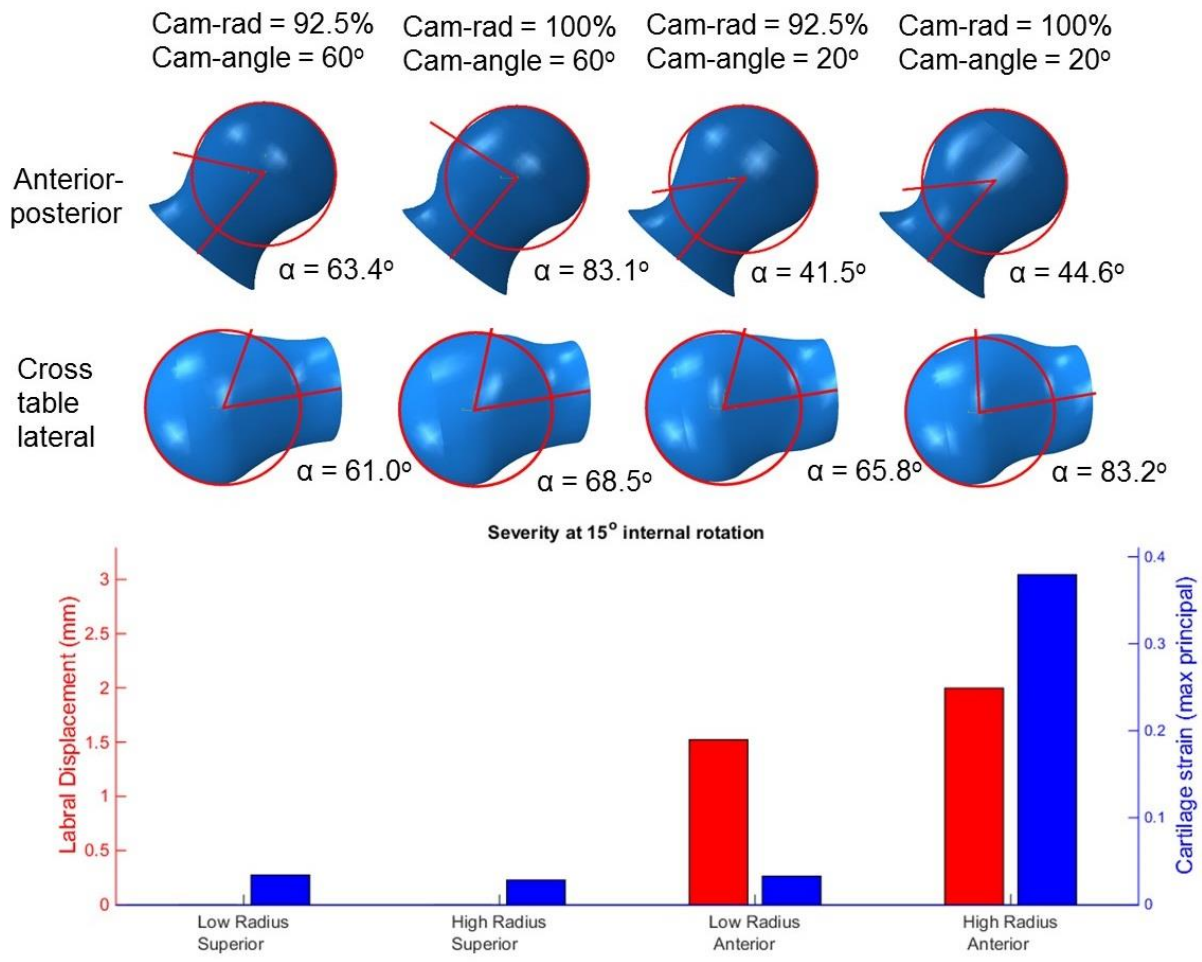


535
 536 **Fig 5:** Illustration of differences between segmented (red) and parametric (blue) models due to
 537 poor local fit. Poor local fit is a result of the best fit ellipse failing to adequately capture
 538 the shape of vertices from a slice of the segmented femoral neck. Parametric model nodes
 539 (pink) at a distance > 1 mm from the nearest segmented model node (black) highlight an
 540 example of poor local fit, leading to higher labral strain and displacement (shown at 20°
 541 internal rotation).

542

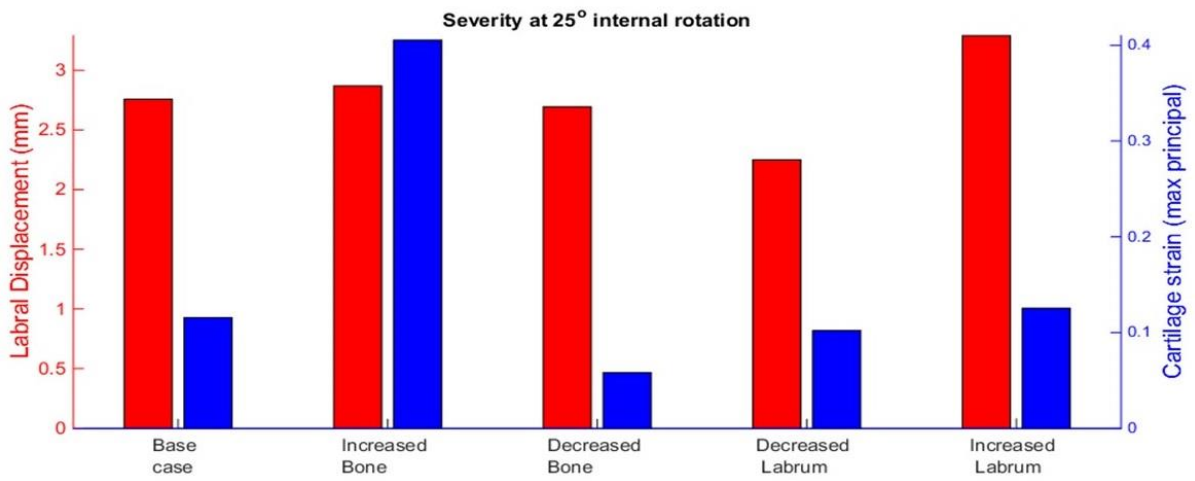
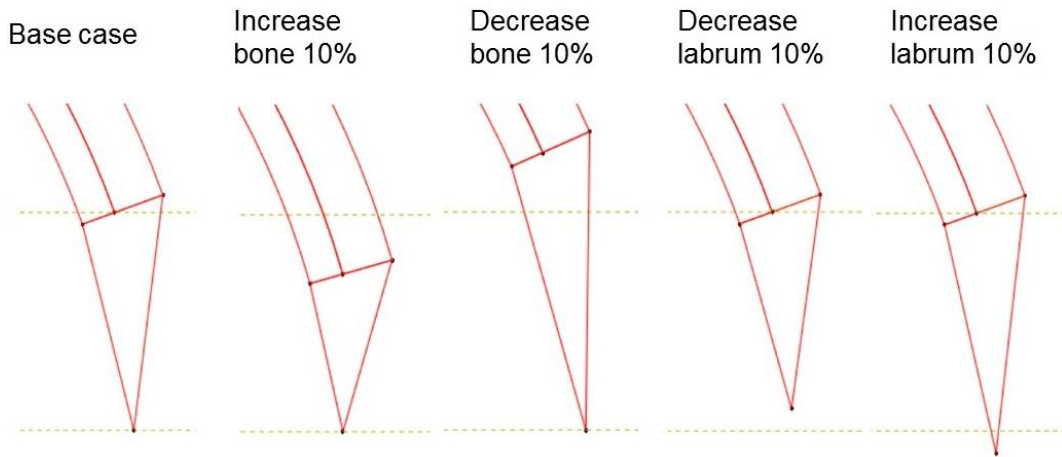
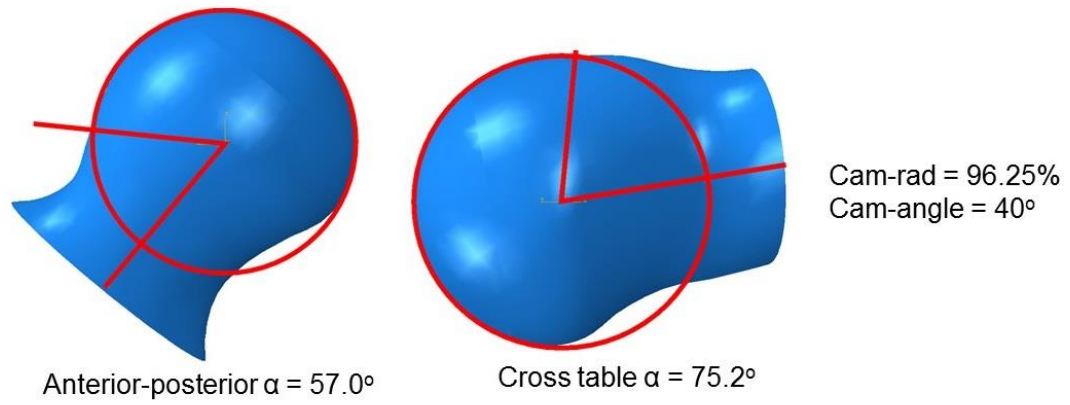
543

544



545

546 **Fig 6:** Labral displacement and cartilage strain for 4 femoral parametric models at 15°
 547 internal rotation and full flexion, with indication of clinical alpha angles. Alpha angles
 548 showed poor correlation to results from parametric models.
 549



550

551

552

553

Fig 7: Labral displacement and cartilage strain for 5 acetabular parametric models at 25° internal rotation and full flexion, with indication of clinical alpha angles. Strain increased with greater bone coverage.